FINAL REPORT

Serial Scanning and Registration of High Resolution Quantitative Computed Tomography Volume Scans for the Determination of Local Bone Density Changes

Robert T. Whalen, Ph.D.
Life Science Division, NASA Ames Research Center

Sandy Napel, Ph.D.
Chye H. Yan, M.S.
Radiology Department, Stanford University

1 November 1996

Introduction

During this 2 years project, we have made great progress in developing the methods required to study bone remodeling as a function of time. The following paragraphs summarizes our accomplishments.

1 CT Acquisition Protocols

During the two year duration of this project, we have performed a number of experiments to determine the best protocol for serial imaging of the calcaneus for quantitative applications. The experiments consisted of the following:

Rob Whalen constructed a phantom that models the calcaneus and its surrounding soft tissue. We scanned the phantom using two different energies (80kVp, 120kVp) and 3 different intensities (80mA, 200mA, 400mA) in both spiral and conventional modes. For each of the 12 combinations of parameters, we obtained 30 scans of the phantom at the same location. We determined the noise level for each combination by computing the standard deviation of the voxels within the center of the calcaneus model across the corresponding 30 scans. The results of these experiments were:

(a) We have selected Spiral CT over conventional CT for the following reasons:
   (1) Spiral CT significantly reduces the inter-slice registration error that usually occurs in Axial CT and therefore results in more accurate surface and volume reconstruction.
   (2) For thin-slice scanning (as we must do in this application), the patient dose in spiral CT is lower compared to conventional for the same longitudinal coverage and technique (kV, mA) factors.
   (3) the availability of overlapping slices leads to reduced partial volume errors which in term improves the accuracy of the surface detection algorithm, crucial for serial registration capability.

(b) We need to scan at 120 kV and 400 mA in order to achieve noise levels low enough to achieve the required precision.

2 Image Registration

We have developed, implemented, and tested a surface registration system by modifying and extending the methods previously developed for multi-modality applications. As the existing system was not optimized for high resolution quantitative computed tomography (QCT), we developed new methodologies to improve the registration accuracy and computation speed:

(a) Surface detection algorithm and representation:
   We have developed a robust and accurate 3-D surface detection algorithm. Our implementation of the algorithm results in a set of surface points and corresponding normals which are stored in a new efficient data structure. The maximum error of our 3-D detection algorithm was 0.2 voxel compared to 0.5 voxel for a conventional detection algorithm. The new surface representation and corresponding data structure improved registration speed by at least 5 times compared to more traditional triangular mesh-generating methods.

(b) Interpolation function:

We have developed a methodology to select the optimal interpolation function based on the noise structure, voxel size and image content. This significantly reduces the computation time and interpolation error incurred in resampling the data volume.

(c) Gold standard:

We initially tested our registration method using an external reference system and related software as a "gold standard." During the course of this work, we discovered that our new methods had residual errors comparable to errors expected from the gold standard registration system. So we developed a new technique for registration using frames that resulted in much higher accuracy. This method, which can be used for any stereotaxic registration application, allows better quantification of the accuracy of frameless registration systems such as ours. As before, it requires the attachment of an external reference system that must be kept in place during and between scanning. However, existing methods that are widely deployed in neurosurgical applications require accurately and precisely constructed frames. In contrast, our method assumes only linear structures in the frame and utilizes all 3D information.

We tested our new "gold standard" using a frame constructed by Robert Whalen at NASA. Registration between pairs of successive scans had a maximum error of 0.1 voxel and an average error of 0.07 voxel [1][2].

We implemented the registration system, including items (a-b) above, together with a user interface on a general purpose workstation. This system requires minimal user intervention, registers CT volumes containing the whole calcaneus (time required to register two 512 x 512 x 80 slice volumes is approx. 2 hr.. on a SparcStation 20) and is now available for routine use in our labs. We scanned 3 calcanei (attached to the Whalen-stereotaxic frame) in different orientations and registered each pair (total of 5 pairs) using the new registration system. Based on the newly developed gold standard, the registration had an average error of 0.7 voxel (0.18mm) and a maximum error of 1.4 voxel (0.36mm). This result clearly showed that the accuracy of the new system is suitable for high resolution QCT [3].

3 CT attenuation accuracy

Beam hardening is caused by filtering of the polychromatic x-ray spectrum by the objects in the scan field. This effect, if not corrected, can cause severe artifacts in CT images and result in inaccurate measures of attenuation. Because we expect bone density in our patient population to change over time, beam filtration will change as well. Therefore, the errors caused by beam filtration will also change, making it difficult to compare bone density from measurements made at different times. We studied the effect that bone density changes have on these errors by scanning a specially constructed phantom consisting of a water-filled cylinder containing in its center a thin aluminum shell filled with solutions of various concentrations of potassium phosphate to simulate different bone densities. We used four different concentrations and 3 different correction techniques with the following results:

(a) Scans using only the standard water correction: Water correction is standard on all CT scanners. However, using it alone resulted in errors caused by beam hardening that are much greater than our accuracy requirements demand.

(b) Scans using the iterative bone option (IBO) correction method: This method is a proprietary algorithm available on General Electric CT scanners that corrects for the spectral hardening caused by the skull in CT scans of the head. The errors caused by beam hardening vary with bone density less than without IBO; however, the errors are still too high on the average.

(c) Scans using a water bolus (with and without IBO): The water bolus pre-hardens the beam before it reaches the phantom to reduce beam hardening error. However, the corresponding increase in noise level reduced the precision of our measurements below our requirements.

4. Publications

Reprints or pre-prints of references below are included in the Appendix.

References

1. Yan CH, Beaupre G, Whalen R, Sumanaweera TS, Napel S. Precise and Accurate Gold Standard for Multimodality and Serial Registration Method Evaluations. Accepted for presentation at the 82nd RSNA, Chicago, IL, 1996.
2. Yan CH, Whalen R, Beaupre G, Sumanaweera TS, Yen SY, Napel S. A New Methodology for Registration Accuracy Evaluation. To be submitted to Nov 96 Medical Physics .
3. Yan CH, Beaupre G, Whalen R, Napel S. Registration of Serial Skeletal Images for Accurately Measuring Changes in Bone Density. Submitted to 43rd Annual Meeting , Orthopaedic Research Society.

APPENDIX

A New Methodology for Registration Accuracy Evaluation

Chye Hwang Yan[1], Robert T. Whalen[2], Gary S. Beaupre[3],
Thilaka S. Sumanaweera[4], Shin Y. Yen[1] and Sandy Napel[5]
Department of [1]Electrical Engineering and [5]Radiology, Stanford University, Stanford, CA
[2]Life Science Division, NASA Ames Research Center, Mountain View, CA
[3]Rehabilitation R&D Center, VA, Palo Alto, CA
[4]Acuson, Mountain View, CA

Abstract

This paper presents a new algorithm for frame registration. Our algorithm requires only that the frame be comprised of straight rods, as opposed to the N structures or an accurate frame model required by existing algorithms. The algorithm utilizes the full 3D information in the frame as well as a least square weighting scheme to achieve highly accurate registration. We use simulated CT data to assess the accuracy of our algorithm. Experimental results show that the proposed algorithm is comparable to the best existing technique with knowledge of the exact frame model. In situations where there is a discrepancy of more than $0.1cm$ (0.2% of the frame dimension) between the frame and the mathematical model, the proposed technique produces registrations that are 2 times more accurate than that from existing techniques. We also outline a routine for estimating the registration error. This allows us to take the uncertainty of the frame registration into consideration during an accuracy evaluation of a frameless registration system. In one test of using the proposed frame registration system as the gold standard to assess the accuracy of a surface-based (frame-less) registration system, error estimates changed by 10% when the estimates of the error in the frame-based system were accounted for.

1 Introduction

Recent advances in medical imaging have led to an increased interest in image registration. Its usage includes stereotaxic surgery, clinical diagnosis, therapy planning, image guided surgery, and many others [1] [2] [3]. Refer to [4] [5] for extensive reviews on registration algorithms.

This work is motivated by our interest in the non-invasive determination of changes in bone mass. Non-invasive measurement of changes in bone apparent density require imaging the same skeletal site at different times and registering the serial images. To this end, we have developed a semi-automatic, 3D surface-based registration technique that does not require the use of an external frame or fiducial markers. we can make non-invasive measurements of changes in bone apparent density. Mis-registration can introduce errors and also limit the size of the measured volume (the effect of mis-registration errors increases as the size of the measured volume decreases). For these reasons, precise evaluation of the registration algorithm accuracy is crucial [6].

The availability of a good method for quantifying registration accuracy (Gold Standard) not only allows researchers to compare their algorithms, but most importantly, it enables system designers to put registration algorithms into practical use with confidence. Current quantification methods can be divided into three major groups: use of 1) computer generated data sets; 2) anatomical landmarks and 3) fiducial markers or frame. In the first method [7] [8], a second image set is generated from an acquired image set by rotating and translating it through a known amount. In this case, the true transformation is known. The drawbacks of this technique are that the second image set has (1) noise correlated with the noise in the first set, and (2) lower spatial resolution than the first due to the interpolation required to generate it. These effects result in conditions that would not be

encountered in actual registration of separately acquired scans. The second method utilizes internal landmarks to evaluate registration algorithms [9] [10]. Registration error is taken as the root-mean-square (rms) distance between corresponding landmarks and is assumed uniform throughout the registered volume. The small number of usable landmarks and the errors associated with landmark detection are the main deficiencies of this method. The last and most popular method [2] [11] [12] [13] [14] [15] [16] [17], assumes that the transformation of externally applied frame/markers is the true transformation. As opposed to anatomical landmarks, the frame/markers are usually constructed in a manner to enable accurate detection.

The gold standard transformation in categories (2) and (3) by itself has registration error associated with it, and that error is commonly ignored. If the error in the gold standard is comparable to that of the algorithm under examination, then the evaluation result is useless. This problem is crucial at locations far away from landmarks/markers/frame as the registration error of the gold standard is likely to change as we move away from these structures (usually the landmarks/markers/frame are not in the VOI). In [11] [12], the authors have tried to address this problem by inserting rods into the VOI (a cadaver brain) and using the distance between corresponding rods as a measure of registration accuracy. This method has good results; however the detection error of the rods are ignored and the quantification is precise only in the region near the rods (not the whole VOI). Also this method is invasive and can only be performed on cadavers. In general, current quantification techniques have two shortcomings: 1) the registration error of the gold standard is ignored, 2) the evaluation is accurate only in the region near the landmarks/markers/frame which does not contain the whole VOI.

The current techniques for frame registration are mainly designed for the field of stereotaxic surgery [13] [14] [15] [18] [19]. In all these techniques, the authors have assumed that the frame is comprised of parallel N structured rods and that an accurate mathematical model of the frame construction is available. Three main shortcomings of these techniques are: 1) registration accuracy depends on the accuracy of the frame construction, 2) they do not utilize the full 3D information in the frame, and 3) they are not generic; ie. they are not applicable to other non-standard frames.

This paper presents a new algorithm for frame registration. Our algorithm only requires that the frame be comprised of a set of straight rods (N structure or exact model are not required), thereby making the algorithm applicable to all type of frames. The algorithm utilizes the full 3D information in the frame and a least square weighting scheme to achieve highly accurate registration. We also present a routine for estimating the registration error.

Section 2 contains an outline of the proposed registration algorithm and the least square weighting scheme. In addition, we define the error measure for registration algorithms comparison and also outline a method for estimating the registration error of our proposed algorithm. Section 3 describes the methods we used to validate our technique. Section 4 contains the report of the the experimental results from Section 3. Finally, the conclusions of our study are presented in Section 5.

2 Registration Algorithm

2.1 Problem Definition

We are given two 3D image sets of a frame. The imaging modality for these images can be the same (acquired at different times) or different (e.g. CT and MR). Our goal is to find a transformation (based on the frame) that will relate the coordinate systems of these image sets. Before we are able to perform any registration, we need to extract the line parameters representing the rods from each image set. There are numerous ways of estimating the line parameters; the technique we used is outlined in Section 3.1.3.

Given the equation of a line L:

$$L: \quad \mathbf{r} = k\mathbf{m} + \mathbf{a}$$

where $\mathbf{m}$ and $\mathbf{a}$ are the gradient and intercept. The equation of a transformed line can be written as

$$L' : \quad \mathbf{r} = k\mathbf{R}\mathbf{m} + \mathbf{R}\mathbf{a} + \mathbf{t}$$

where the transformation is comprised of a rotation $\mathbf{R}$ followed by a translation $\mathbf{t}$. Note that any rigid body transformation can be expressed in terms of $\mathbf{R}$ and $\mathbf{t}$. Next, we represent a set of l lines by $(\mathbf{M}, \mathbf{A}, \mathbf{\Omega}_m, \mathbf{\Omega}_a)$ by

$$\begin{aligned} \mathbf{M} &= (\mathbf{m}_1, \mathbf{m}_2, \cdots, \mathbf{m}_l) \\ \mathbf{A} &= (\mathbf{a}_1, \mathbf{a}_2, \cdots, \mathbf{a}_l) \\ \mathbf{\Omega}_m &= (\Sigma_{m1}, \Sigma_{m2}, \cdots, \Sigma_{ml}) \\ \mathbf{\Omega}_a &= (\Sigma_{a1}, \Sigma_{a2}, \cdots, \Sigma_{al}) \end{aligned}$$

where $\mathbf{m}_i$ and $\mathbf{a}_i$ are the gradient and intercept of the *ith* line. The estimation error of $\mathbf{m}_i$ and $\mathbf{a}_i$ are captured in Σ_{mi} and Σ_{ai} respectively with

$$\begin{aligned} \Sigma_{mi} &= E\{(\mathbf{m}_i - E(\mathbf{m}_i))(\mathbf{m}_i - E(\mathbf{m}_i))^T\} \\ \Sigma_{ai} &= E\{(\mathbf{a}_i - E(\mathbf{a}_i))(\mathbf{a}_i - E(\mathbf{a}_i))^T\} \end{aligned}$$

We further assume that the estimation errors for each line are unbiased and independent of those for all other lines. So mathematically, the problem can be restated as:

- given two sets of lines $(\mathbf{M}_1, \mathbf{A}_1, \mathbf{\Omega}_{m,1}, \mathbf{\Omega}_{a,1})$ and $(\mathbf{M}_2, \mathbf{A}_2, \mathbf{\Omega}_{m,2}, \mathbf{\Omega}_{a,2})$
- find a transformation $(\mathbf{R}^*, \mathbf{t}^*)$ that *optimally* matches lines in the first set to their corresponding lines in the second set.

2.2 Determining the Rotation and Translation

We divide the transformation determination problem into two subproblems:

- Determine the rotation $\mathbf{R}^*$ using the following criterion:

$$\mathbf{R}^* = \arg\min_{\mathbf{R}} \sum_{i=1}^{l} \| \mathbf{m}_{i,1} - \mathbf{R}\mathbf{m}_{i,2} \|_2^2 \qquad \text{subject to } \mathbf{R}^T\mathbf{R} = \mathbf{I} \tag{1}$$

  where $\mathbf{m}_{i,j}$ is the *ith* column of $\mathbf{M}_j$.

- Determine then the translation under the following scenario:
  We perform a transformation of $(\mathbf{R}^*, \mathbf{t})$ on $(\mathbf{M}_2, \mathbf{A}_2, \mathbf{\Omega}_{m,2}, \mathbf{\Omega}_{a,2})$ to obtain $(\mathbf{M'}_2, \mathbf{A'}_2(\mathbf{t}), \mathbf{\Omega'}_{m,2}, \mathbf{\Omega'}_{a,2})$. For each line L_i in $(\mathbf{M}_1, \mathbf{A}_1, \mathbf{\Omega}_{m,1}, \mathbf{\Omega}_{a,1})$ and its corresponding pair $L'_i(\mathbf{t})$ from $(\mathbf{M'}_2, \mathbf{A'}_2(\mathbf{t}), \mathbf{\Omega'}_{m,2}, \mathbf{\Omega'}_{a,2})$, we define a plane π_i which passes through the centroid of the VOI and is perpendicular to L_i, as shown in Figure 1. We define $\mathbf{p}_i$ as the intersection point of L_i and the plane π_i. Similarly, $\mathbf{p'}_i(t)$ is the intersection point of $L'_i(\mathbf{t})$ and π_i. The optimal translation $\mathbf{t}^*$ is determined by the following criterion:

$$\mathbf{t}^* = \arg\min_{\mathbf{t}} \sum_{i=1}^{l} \| \mathbf{p}_i - \mathbf{p'}_i(\mathbf{t}) \|_2^2 \,. \tag{2}$$

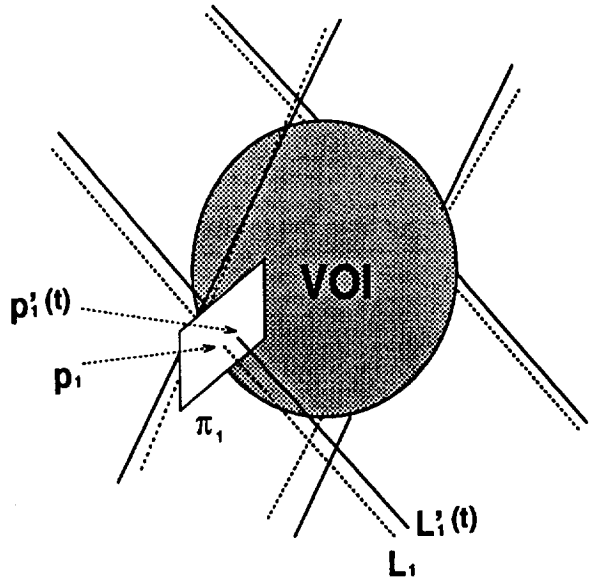

Figure 1: The optimizing criterion for translation

The optimizing rotation for Equation (1) is

$$\mathbf{R}^* = \mathbf{U}\mathbf{V}^T \tag{3}$$

where $\mathbf{U}$ and $\mathbf{V}$ are the unitary matrices in the singular value decomposition of $\mathbf{M}_1\mathbf{M}_2^T$ which is given by

$$\mathbf{U}^T\mathbf{M}_1\mathbf{M}_2^T\mathbf{V} = diag(\lambda_1, \lambda_2, \lambda_3) = \Lambda$$

Refer to Appendix A for a detailed derivation. In Appendix B, we show that Equation (2) is equivalent to a quadratic optimization problem and can be solved by using the calculus of variation. The optimizing translation is

$$\mathbf{t}^* = \{\sum_{i=1}^{l}(\mathbf{I} + \frac{1}{(\mathbf{n}_i.\mathbf{m'}_i)^2}\mathbf{n}_i\mathbf{n}_i^T - \frac{1}{\mathbf{n}_i.\mathbf{m'}_i}\mathbf{m'}_i\mathbf{n}_i^T - \frac{1}{\mathbf{n}.\mathbf{m'}_i}\mathbf{n'}_i\mathbf{m'}_i^T)\}^{-1}\sum_{i=1}^{l}(\frac{\mathbf{k}_i.\mathbf{m'}_i}{\mathbf{n}_i.\mathbf{m'}_i}\mathbf{n}_i - \mathbf{k}_i). \tag{4}$$

2.3 Weighting Scheme for $\mathbf{R}^*$ and $\mathbf{t}^*$

In Section 2.2, we have formulated the optimization criteria based on the assumption that the line estimation error variances are equal. In cases where Ω_m, and Ω_a are available and the error variances are not constant, we could improve the accuracy of the frame registration by using a weighting scheme. In this method, we weight the registration error of each line by a weight chosen inversely proportional to their estimation error variances. We reformulate Equation (1) and (2) as

$$\mathbf{R}^* = \arg\min_{\mathbf{R}} \sum_{i=1}^{l} w_{Ri} \parallel \mathbf{m}_{i,1} - \mathbf{R}\mathbf{m}_{i,2} \parallel_2^2 \qquad \text{subject to } \mathbf{R}^T\mathbf{R} = \mathbf{I} \tag{5}$$

and

$$\mathbf{t}^* = \arg\min_{\mathbf{t}} \sum_{i=1}^{l} w_{ti} \parallel \mathbf{p}_i - \mathbf{p'}_i(\mathbf{t}) \parallel_2^2 \tag{6}$$

with

$$\begin{aligned}\frac{1}{w_{Ri}} &= E(\| \mathbf{m}_{i,1} - \mathcal{R}\mathbf{m}_{i,2} \|_2^2) \\ \frac{1}{w_{ti}} &= E(\| \mathbf{p}_i - \mathbf{p'}_i(\mathcal{T}) \|_2^2)\end{aligned}$$

where $(\mathcal{R}, \mathcal{T})$ is the true transformation. Appendix C shows the procedure for calculating w_{Ri} and w_{ti}. Equation (5) and (6) can be solved using the procedures in Appendix A and B.

2.4 Error Measure

Before we could perform any comparison between registration systems, we need to define the error measure that is to be used in the comparison. Let the true transformation be $(\mathcal{R}, \mathcal{T})$. For any other transformation $(\mathbf{R}, \mathbf{t})$, the registration error at a point $\mathbf{p}$ is

$$\delta = (\mathcal{R} - \mathbf{R})\mathbf{p} + (\mathcal{T} - \mathbf{t}).$$

By using the triangle inequality, we have

$$\begin{aligned}E(\| \delta \|_2) &\leq E(\| \tilde{\mathbf{R}}\mathbf{p} \|_2) + E(\| \tilde{\mathbf{t}} \|_2) \\ &\leq E(|\lambda_{max}|) \| \mathbf{p} \|_2 + E(\| \tilde{\mathbf{t}} \|_2)\end{aligned}$$

where $\tilde{\mathbf{R}} = \mathcal{R} - \mathbf{R}$, $\tilde{\mathbf{t}} = \mathcal{T} - \mathbf{t}$ and $|\lambda_{max}|$ is the largest absolute eigenvalue of $\tilde{\mathbf{R}}$. $E(|\lambda_{max}|)$ and $E(\| \tilde{\mathbf{t}} \|_2)$ are good indicators for the rotational and translational registration accuracy respectively. Thus we use $(E(|\lambda_{max}|)$, $E(\| \tilde{\mathbf{t}} \|_2))$ as an error measure for comparing registration algorithms. We denote $E(|\lambda_{max}|)$ by ϵ_R and $E(\| \tilde{\mathbf{t}} \|_2)$ by ϵ_t. Note that the translational error in a registration is constant throughout the VOI and its expected value is equal to ϵ_t. Whereas, the rotational error increases linearly with the distance from the center of rotation and a multiplicative constant of ϵ_R. Thus the overall accuracy of a registration algorithm depends on the value of (ϵ_R, ϵ_t) and the size of the VOI. We refer (ϵ_R, ϵ_t) as the frame registration error with rotational registration error ϵ_R and translational registration error ϵ_t.

In actual situations, we do not have the luxury of performing many runs of registration to obtain an estimate for frame registration error. However, it will be extremely useful for us to know the degree of uncertainty in the frame registration. Due to the nice properties of $E(\tilde{\mathbf{R}}^T\tilde{\mathbf{R}})$ and $E(\| \tilde{\mathbf{t}} \|_2^2)$, we outline their derivations in Appendix D. We then approximate ϵ_R with the largest eigenvalue of $E(\tilde{\mathbf{R}}^T\tilde{\mathbf{R}})^{\frac{1}{2}}$ and ϵ_t with $E(\| \tilde{\mathbf{t}} \|_2^2)^{\frac{1}{2}}$.

3 Experimental Design

3.1 Registration Accuracy Comparison

In this section, we compare our technique with two other commonly used techniques. We denote the first technique as the Parallel-N technique [13] and the second as the Point-Based technique [15] [18] [19]. The Parallel-N technique uses 2 detected N-structures as the coordinate system and the Point-Based technique matches each 2D slice separately to an N-bar model.

3.1.1 Simulation

Simulated CT data of a frame, shown in Figure 2(a), were obtained by a simulation program [20]. All CT images (512x512 pixels) were simulated with the following parameters: Axial, 80kV, 100mA, 0.3x0.3x1.0 cm^3 voxels. Figure 2(b) shows a slice from the simulated CT volume. The variance of the poisson noise was experimentally adjusted to be similar to that in an actual scan acquired and reconstructed using the identical parameters.

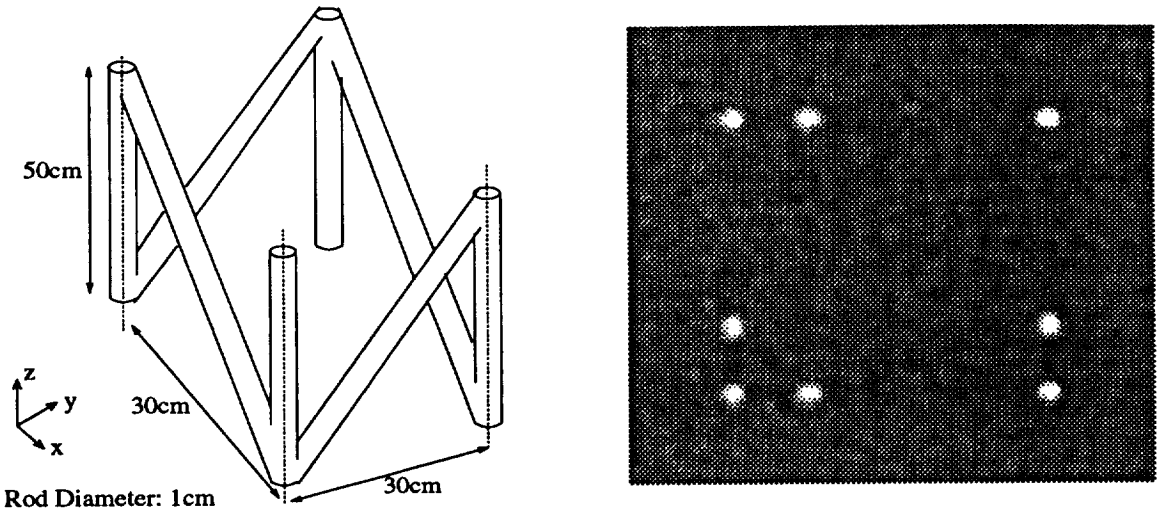

Figure 2: (a) The frame model used in the simulation. (b) A slice of the CT scans.

3.1.2 Data

Sixty contiguous 1.0cm slices were generated from $z = -5cm$ to $z = 55cm$ with the frame in the orientation shown in Figure 2(a). We denoted these sixty slices as a CT volume of the frame. We simulated 50 CT volumes separately such that the noise in each CT volume was independent of those in other CT volumes. We then transformed the model of the frame by a rotation R=(5° about x, 5° about y and 15° about z) and a translation t=(-1.5cm, 1.5cm, -1.5cm). Another set of 50 CT volumes were obtained with the frame in the new orientation.

3.1.3 Methods

For every slice, we used an edge detection algorithm to detect the circumference of the rod [12]. We then performed a least square fit of the circumference to an ellipse. The center of the ellipse was taken to be the center of the rod. Using this method, we estimated the center of the rod in every slice. The parameters of the line representing the rod, $(\mathbf{m}, \mathbf{a}, \Sigma_m, \Sigma_a)$ were estimated using the procedures described in Appendices E and F. For each registration technique, we performed 50 registrations and compared the results obtained with the known true transformation. The exact frame model was used in both the Point-Based and Parallel-N techniques.

For every registration, we used the procedures in Appendix D to obtain $E(\tilde{\mathbf{R}}^T\tilde{\mathbf{R}})$ and $E(\| \tilde{\mathbf{t}} \|)$. We then estimated the frame registration error (ϵ_R, ϵ_t) and compared it with the true value obtained from the previous experiment.

To study the sensitivity of the Parallel-N and the proposed technique to model inaccuracies (the frame and its model do not match), we repeated the experiment with an inaccurate frame. We formed an inaccurate frame by perturbing the end points of all the rods in the frame with a gaussian random variable (with variance σ_n). A 50 CT volume set was obtained using this frame in the orientation shown in Figure 2(a). A the second set was obtained with the inaccurate frame in the second orientation, as in Section 3.1.2. We performed 50 registrations using each registration technique and compared the results with the true transformation. We performed 50 monte carlo simulations for each σ_n ranging from (0.0001cm to 0.2cm).

Method	ϵ_R	ϵ_t (cm)
Point-Based	0.0074 ± 0.000024	0.7167 ± 0.00037
Parallel-N	0.0006 ± 0.000004	0.0074 ± 0.00007
Proposed	0.0009 ± 0.000006	0.0053 ± 0.00004

Table 1: This table shows the expected registration errors (rotation $|\lambda_{max}|$ and translation $\| \tilde{\mathbf{t}} \|$) in the various techniques. (voxel size: 0.3x0.3x1.0 cm^3).

3.2 Evaluation of the Surface-Based Registration Algorithm

We used the proposed frame registration system to evaluate the accuracy of the surface-based registration system that we have customized from [11] for quantifying bone loss over time. We secured excised human calcanei within a custom made fiducial frame shown in Figure 3. We scanned the frame/calcaneus in different orientations. Scanning was done at a resolution of 0.25x0.25x0.5mm^3. The rods in the image volume were extracted by the procedure described in Section 3.1.3. We determined the accuracy of the surface registration algorithm by 1) obtaining the frame transformation using our proposed algorithm, 2) obtaining a transformation for the calcaneus using surface-based algorithm, 3) transforming all calcaneus voxels using both the frame's and the surface's transformation, 4) calculating the distance (error) between corresponding voxels in the two transformed calcaneus images. Note that none of the current frame registration techniques is applicable to this custom-made frame. To examine the effects of noise and contrast, we repeated the whole experiment with the frame/calcaneus immersed in a water bath.

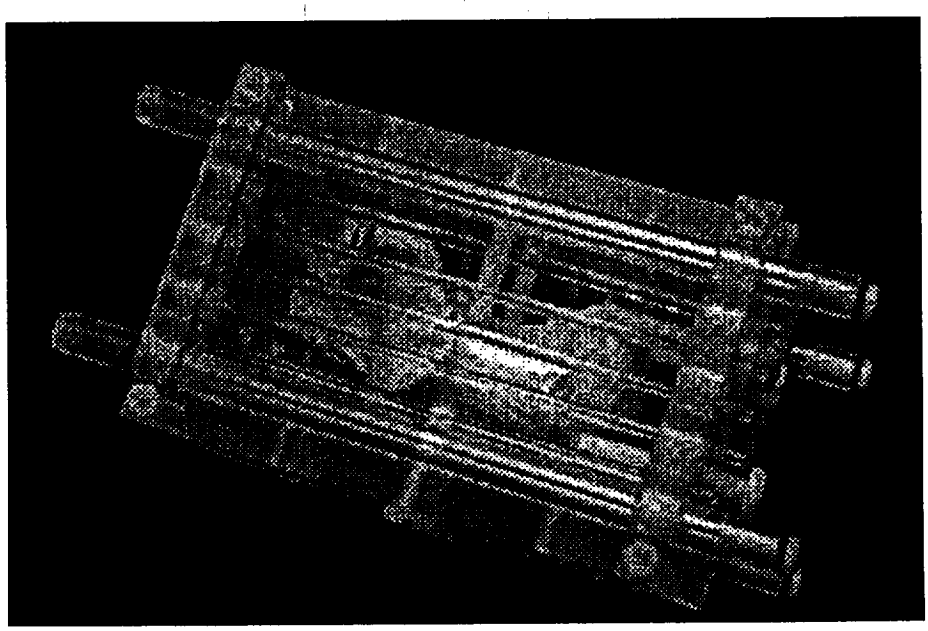

Figure 3: An excised human calcaneus tightly secured in the custom made frame.

4 Results

4.1 Registration Accuracy Comparison

For each registration, we obtain $(\tilde{\mathbf{R}}, \tilde{\mathbf{t}})$ which is used for calculating $(\|\lambda_{max}\|, \|\tilde{\mathbf{t}}\|)$. The mean of $(\|\lambda_{max}\|, \|\tilde{\mathbf{t}}\|)$ from the 50 registration runs is used as an estimate for (ϵ_R, ϵ_t). The results are tabulated in Table 1. As the Point-Based method only utilizes points information on a single slice to perform the registration, its performance is not as good when compared to methods that utilize the entire line. The results show that the performance of the proposed method is comparable to that of Parallel-N method. The proposed method produces a better translational registration while the Parallel-N method is more accurate in rotational registration. The amount of information contained in the true frame model and six rods (four vertical, two slanted) enables the Parallel-N method to produce a better rotational registration than the proposed method whose registration is solely based on the information from eight rods (four vertical, four slanted). However for translational registration, the z-axis translation (refer to Figure 2(a)) can only be determined by slanted rods. In the proposed method, the use of two additional slanted rods provides substantial amount of information on the z-axis translation which leads to a more accurate translational registration in the z-axis. The significant gain in the z-axis translational registration accuracy results in a better overall translational registration for the proposed method. For the simulation, the mean absolute translational registration error in (x-axis, y-axis, z-axis) for the proposed and the Parallel-N methods are $(0.0026, 0.0021, 0.0032)$ and $(0.0020, 0.0026, 0.0060)$ respectively. Note that the proposed method is two times more accurate than the Parallel-N method in the z-axis translational registration.

The estimated values of ϵ_R and ϵ_t are 0.00094 ± 0.000037 and 0.0061 ± 0.00013 respectively. A comparison of these figures with Table 1 shows that there is bias of 0.00004 in the estimate of ϵ_R and 0.0008 in the estimate of ϵ_t. Due to the fact that $E(X^2) \geq E(|X|)^2$ for any random variable X, the approximation done in Section 2.4 introduces a positive bias into the estimates. As we are going to use these estimates to form an upper bound for the registration error of the proposed algorithm, the biases are not significance since they are small (less than 15% of the true value) and positive.

Figure 4 shows the performance of the Parallel-N and the proposed techniques on an inaccurate frame. The accuracy of the Parallel-N technique is degraded with the increase in frame-model discrepancies. Whereas the performance of the proposed technique, which is not based on any frame model, is not affected by the frame-model discrepancies. If the mis-match between the frame and the model is more than $0.01cm$, the registration error for the Parallel-N technique increases exponentially. The performance of the proposed technique surpass that of the Parallel-N technique, in both rotational and translational aspect, when the frame-model discrepancies are more than $0.05cm$ (0.1% of the frame dimension). This amount of discrepancies are common in practice which may due to the frame being dropped or damaged or mal-machined.

4.2 Evaluation of the Surface-Based Registration Algorithm

Figure 5(a) shows an error plot for a slice of the calcaneus (in air) using the frame-based transformation as truth. The availability of the estimated $(\tilde{\mathbf{R}}, \tilde{\mathbf{t}})$ allows us to account for the frame registration error in our evaluation. By the triangle inequality, we have

$$\textit{registration error}\,|_{true} \leq \textit{registration error}\,|_{frame} + \textit{frame registration error.}$$

Thus by adding the estimated frame registration error to the error in Figure 5(a), we have formed an upper bound for the true registration error of the surface-based algorithm. Figure 5(b) shows the registration error (*with respect to the true transformation*) of the surface algorithm for that particular slice.

By repeating the same analysis for the rest of the calcaneus, we have obtained an worst case error map for the surface-based technique on the whole calcaneus. Table 2 shows a performance summary for our surface-based algorithm. Note that there is a significant increase in registration error (10%) when the frame registration uncertainty is taken into consideration.

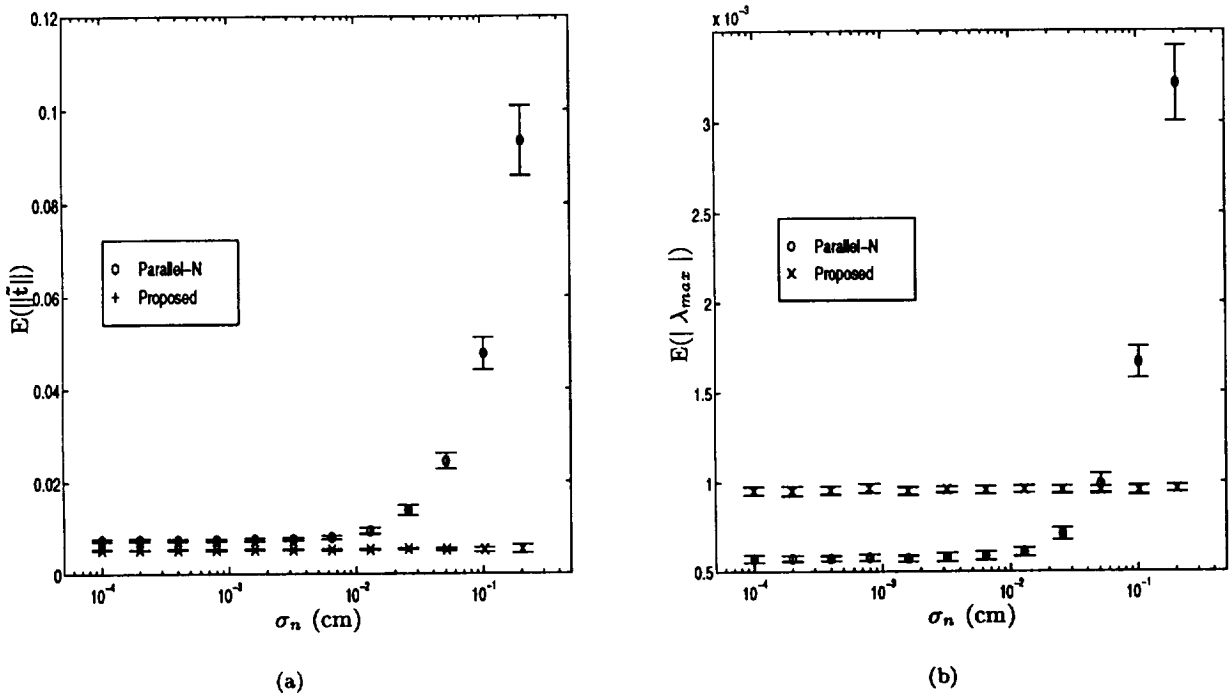

Figure 4: This figure shows the effects of frame model discrepancies on the performance of the Parallel-N and the proposed method. (a) The translation error $E(\|\tilde{t}\|)$ plotted against the perturbation σ_n (the standard deviation of the gaussian perturbation). (b) The rotation error $E(|\lambda_{max}|)$ plotted against the perturbation σ_n. The horizontal lines are 1 standard deviation from the mean. (voxel size: 0.3x0.3x1.0 cm^3)

	Error (mm) relative to Frame			Error (mm) true		
	Min	Ave	Max	Min	Ave	Max
Calcaneus in Air	0.002	0.18	0.36	0.015	0.20	0.39
Calcaneus in Water	0.040	0.20	0.40	0.055	0.22	0.43

Table 2: This table shows the evaluation results for the surface-based algorithm. The first set of results is obtained under the assumption that the frame registration represents the true transformation. The second set of results accounts for the uncertainty in the frame registration

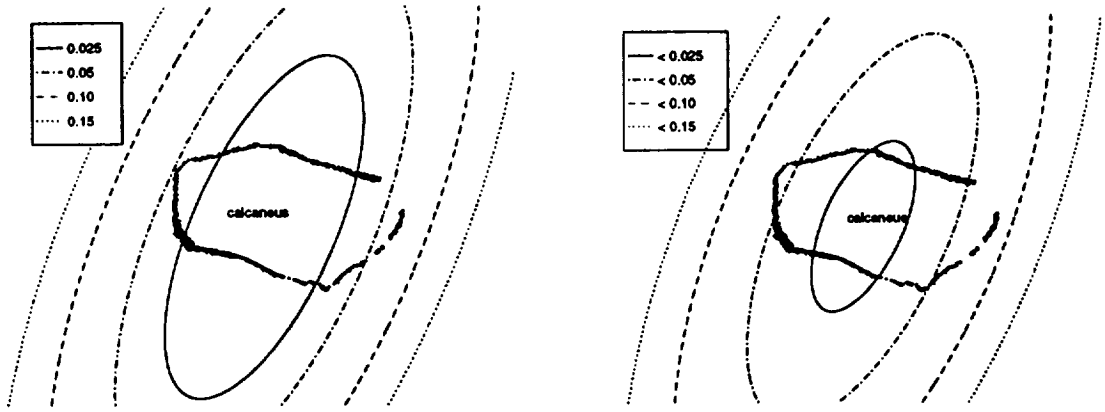

(a) (b)

Figure 5: This figure shows the contour plot of the registration error on a slice (through the centroid of the VOI) from the image volume. (a) shows the registration error with the frame's registration assumed to be the true registration. (b) shows the registration error when the uncertainty of the frame registration is taken into consideration

5 Conclusion

We have described an accurate frame registration algorithm. The proposed algorithm assumes only linear structures (rods) in the frame and also utilizes all the 3D information to perform the registration. The proposed method is not restricted to the head frame (which is comprised of N-structures). So to perform registration system accuracy evaluations on a VOI other than the head, one only needs to designate some linear structures as the frame. A comparison with various current frame registration algorithms shows that the proposed method is more robust and more accurate. In addition, we have derived an estimator for the frame registration error. We have shown that it is necessary to incorporate frame registration errors into the evaluation of frame-less registration system and that doing so gives an upper bound on the expected error of the frame-less system.

6 Acknowledgments

This research was funded primarily by NASA through NASA Cooperative Agreement NCC-5088 and the Department of Veterans Affairs through Merit Review project B802-RA. In addition, we acknowledge addition support from the National Institutes of Health (P41 RR09784), the Lucas Foundation and the Phil N. Allen Trust. The authors would like to thank C.R. Crawford for the CT simulation program and Laura Logan for her technical assistance.

A Determining the Rotation R*

Given two matrices $\mathbf{M}_1$ and $\mathbf{M}_2$, we would like to find a rotation matrix $\mathbf{R}^*$ such that

$$\mathbf{R}^* = \arg\min_{\mathbf{R}} \sum_{i=1}^{l} \| \mathbf{m}_{i,1} - \mathbf{R}\mathbf{m}_{i,2} \|_2^2 \qquad \text{subject to } \mathbf{R}^T\mathbf{R} = \mathbf{I}$$

The above optimizing criterion can be written as

$$\mathbf{R}^* = \arg\min_{\mathbf{R}} \| \mathbf{M}_1 - \mathbf{R}\mathbf{M}_2 \|_F^2 \qquad \text{subject to } \mathbf{R}^T\mathbf{R} = \mathbf{I} \tag{7}$$

where $\|.\|_F$ is the Frobenius norm [21]. Since $\mathbf{R}$ is orthogonal, then

$$\| \mathbf{M}_1 - \mathbf{R}\mathbf{M}_2 \|_F^2 = trace(\mathbf{M}_1^T\mathbf{M}_1) + trace(\mathbf{M}_2^T\mathbf{M}_2) - 2trace(\mathbf{R}^T\mathbf{M}_1\mathbf{M}_2^T)$$

then (7) is equivalent to the problem of maximizing $trace(\mathbf{R}^T\mathbf{M}_1\mathbf{M}_2^T)$. The maximizing $\mathbf{R}$ can be found by calculating the singular value decomposition (SVD) of $\mathbf{M}_1\mathbf{M}_2^T$. If

$$\mathbf{U}^T\mathbf{M}_1\mathbf{M}_2^T\mathbf{V} = diag(\lambda_1, \lambda_2, \lambda_3) = \Lambda \tag{8}$$

is the SVD decomposition, then

$$\begin{aligned} trace(\mathbf{R}^T\mathbf{M}_1\mathbf{M}_2^T) &= trace(\mathbf{R}^T\mathbf{U}\Lambda\mathbf{V}^T) \\ &= trace(\mathbf{V}^T\mathbf{R}^T\mathbf{U}\Lambda) \\ &= z_{11}\lambda_1 + z_{22}\lambda_2 + z_{33}\lambda_3 \end{aligned}$$

where $\mathbf{Z} = \mathbf{V}^T\mathbf{R}^T\mathbf{U}$ and z_{ij} is the (i,j) element of $\mathbf{Z}$. As $\mathbf{U}$ and $\mathbf{V}$ are unitary, the upper-bound is obtained by setting $\mathbf{Z} = \mathbf{I}$. Thus $\mathbf{R}^* = \mathbf{U}\mathbf{V}^T$ [21].

B Determining the Translation t*

Let the planes assigned to each line be $(\pi_1, \pi_2, \cdots, \pi_l)$. The point of intersection of a line $L : \mathbf{r} = \mathbf{a} + k\mathbf{m}$ and a plane $\pi : \mathbf{r}.\mathbf{n} = d$ is given by

$$\mathbf{p} = \frac{d - \mathbf{a}.\mathbf{n}}{\mathbf{m}.\mathbf{n}}\mathbf{m} + \mathbf{a}. \tag{9}$$

Similarly, the intersection of the plane and a line with a translation $\mathbf{t}$, $L : \mathbf{r} = \mathbf{a} + \mathbf{t} + k\mathbf{m}$, is given by

$$\mathbf{p}(\mathbf{t}) = \frac{d - \mathbf{a}.\mathbf{n}}{\mathbf{m}.\mathbf{n}}\mathbf{m} + \mathbf{a} - \frac{\mathbf{t}.\mathbf{n}}{\mathbf{m}.\mathbf{n}}\mathbf{m} + \mathbf{t}.$$

So the minimization problem

$$\mathbf{t}^* = \arg\min_{\mathbf{t}} \sum_{i=1}^{l} \| \mathbf{p}_i - \mathbf{p'}_i(\mathbf{t}) \|_2^2$$

can be written as

$$\mathbf{t}^* = \arg\min_{\mathbf{t}} \sum_{i=1}^{l} \| \mathbf{k}_i - \frac{\mathbf{t}.\mathbf{n}_i}{\mathbf{m'}_i.\mathbf{n}_i}\mathbf{m'}_i + \mathbf{t} \|_2^2 \tag{10}$$

with

$$\begin{aligned}
\mathbf{a'}_i &= \mathbf{R}^*\mathbf{a}_{i,2}, \\
\mathbf{m'}_i &= \mathbf{R}^*\mathbf{m}_{i,2} \\
\mathbf{k}_i &= \frac{d_i - \mathbf{a'}_i.\mathbf{n}_i}{\mathbf{m'}_i.\mathbf{n}_i}\mathbf{m'}_i + \mathbf{a'}_i - \frac{d_i - \mathbf{a}_i.\mathbf{n}_i}{\mathbf{m}_i.\mathbf{n}_i}\mathbf{m}_i - \mathbf{a}_i
\end{aligned}$$

where $\mathbf{m}_{i,2}$ and $\mathbf{a}_{i,2}$ are the gradient and intercept of the *ith* line in $(\mathbf{M}_2, \mathbf{A}_2, \mathbf{\Omega}_{m,2}, \mathbf{\Omega}_{a,2})$. Equation (10) is a quadratic minimization problem and $\mathbf{t}^*$ can be found by the calculus of variation. At the stationary point, we have

$$\sum_{i=1}^{l}(\mathbf{I} + \frac{1}{(\mathbf{n}_i.\mathbf{m'}_i)^2}\mathbf{n}_i\mathbf{n}_i^T - \frac{1}{\mathbf{n}_i.\mathbf{m'}_i}\mathbf{m'}_i\mathbf{n}_i^T - \frac{1}{\mathbf{n}.\mathbf{m'}_i}\mathbf{n'}_i\mathbf{m'}_i^T)\mathbf{t}^* = \sum_{i=1}^{l}(\frac{\mathbf{k}_i.\mathbf{m'}_i}{\mathbf{n}_i.\mathbf{m'}_i}\mathbf{n}_i - \mathbf{k}_i). \tag{11}$$

With this equation, $\mathbf{t}^*$ can be found by a matrix inversion.

C Determining the weights

Since the errors in $\mathbf{m}$ are unbiased and independent, we can show that at the true rotation $\mathcal{R}$,

$$\begin{aligned}
E(\mathbf{m}_{i,1} - \mathcal{R}\mathbf{m}_{i,2}) &= \mathbf{0} \\
E(\| \mathbf{m}_{i,1} - \mathcal{R}\mathbf{m}_{i,2} \|_2^2) &= trace(\Sigma_{mi,1}) + trace(\Sigma_{mi,2}) \\
&= \frac{1}{w_{Ri}^2}
\end{aligned}$$

Similarly, with the assumption that the errors incurred in the line fitting procedure are unbiased and independent, at true transformation $(\mathcal{R}, \mathcal{T})$ we have

$$\begin{aligned}
E(\mathbf{p}_i - \mathbf{p'}_i(\mathcal{T})) &= \mathbf{0} \\
E(\| \mathbf{p}_i - \mathbf{p'}_i(\mathcal{T}) \|_2^2) &= E(\| \mathbf{p}_i - \overline{\mathbf{p}_i} \|_2^2) + E(\| \mathbf{p'}_i(\mathcal{T}) - \overline{\mathbf{p'}_i(\mathcal{T})} \|_2^2)
\end{aligned}$$

From (9), we have

$$\begin{aligned}
E(\| \mathbf{p} - E(\mathbf{p}) \|_2^2) &= E(\| \mathbf{a} - \bar{\mathbf{a}} - \frac{(\mathbf{a} - \bar{\mathbf{a}}).\mathbf{n}}{\mathbf{m}.\mathbf{n}}\mathbf{m} \|_2^2) \\
&= E(\| \tilde{\mathbf{a}} - \frac{\tilde{\mathbf{a}}.\mathbf{n}}{\mathbf{m}.\mathbf{n}}\mathbf{m} \|_2^2) \\
&= E(\| (\mathbf{I} - \frac{\mathbf{m}\mathbf{n}^T}{\mathbf{m}.\mathbf{n}})\tilde{\mathbf{a}} \|_2^2 \\
&= E(\tilde{\mathbf{a}}^T(\mathbf{I} - \frac{\mathbf{m}\mathbf{n}^T}{\mathbf{m}.\mathbf{n}})(\mathbf{I} - \frac{\mathbf{n}\mathbf{m}^T}{\mathbf{m}.\mathbf{n}})\tilde{\mathbf{a}}) \\
&= E(\tilde{\mathbf{a}}^T\Theta\tilde{\mathbf{a}}) \qquad \text{where } \Theta = (\mathbf{I} - \frac{\mathbf{m}\mathbf{n}^T}{\mathbf{m}.\mathbf{n}})(\mathbf{I} - \frac{\mathbf{n}\mathbf{m}^T}{\mathbf{m}.\mathbf{n}}) \\
&= \sum_{ij}(\Theta)_{ij}(\Sigma_{ai,1})_{ij}
\end{aligned}$$

Using a similar procedure, we obtain

$$\begin{aligned}
E(\| \mathbf{p'}_i(\mathbf{t}^*) - \overline{\mathbf{p'}_i(\mathbf{t}^*)} \|_2^2) &= \sum_{ij}(\mathcal{R}^T\Theta\mathcal{R})_{ij}(\Sigma_{ai,2})_{ij} \\
&\approx \sum_{ij}(\mathbf{R}^{*\mathbf{T}}\Theta\mathbf{R}^*)_{ij}(\Sigma_{ai,2})_{ij}
\end{aligned}$$

Thus, combining these results, we have

$$\frac{1}{w_{ti}} \approx \sum_{ij}(\Theta)_{ij}(\Sigma_{ai,1})_{ij} + \sum_{ij.}(\mathbf{R}^{*\mathbf{T}}\Theta\mathbf{R}^{*})_{ij}(\Sigma_{ai,2})_{ij}.$$

D Derivation of the Registration Error Estimators

D.1 Uncertainty in Rotation

Without loss in generality, we assume that $\mathbf{M}_2$ is measured exactly and its detection errors are transfered to the respective rods in $\mathbf{M}_1$. Based on this assumption, we have

$$\begin{aligned}\mathbf{M}_1 &= \mathcal{R}\mathbf{M}_2 + \tilde{\mathbf{M}}_1 - \mathcal{R}\tilde{\mathbf{M}}_2 \\ &= \mathcal{R}\mathbf{M}_2 + \Delta\end{aligned}$$

where $\mathcal{R}$ is the true rotation. Our aim is to find a formula for

$$E(\tilde{\mathbf{R}}^T\tilde{\mathbf{R}}) = E\{(\mathbf{R}^* - \mathcal{R})^T(\mathbf{R}^* - \mathcal{R})\}. \tag{12}$$

where $\mathbf{R}^* = \mathbf{U}\mathbf{V}^T$. Since we have no access to $\mathcal{R}$, we could treat $\mathcal{R}$ as a small perturbation from $\mathbf{R}^*$. Following the derivation of $\mathbf{R}^*$, let $\mathcal{R} = \mathcal{U}\mathcal{V}^T$. It can be shown that $\mathbf{U}, \mathbf{V}, \mathcal{U}, \mathcal{V}$ are the eigenvectors of $\mathbf{A}$, $\mathbf{B}$, $\mathbf{A}+\mathbf{E}$ and $\mathbf{B}+\mathbf{F}$ respectively, where

$$\begin{aligned}\mathbf{A} &= \mathbf{M}_1\mathbf{M}_2^T\mathbf{M}_2\mathbf{M}_1^T, \quad \mathbf{B} = \mathbf{M}_2\mathbf{M}_1^T\mathbf{M}_1\mathbf{M}_2^T, \\ \mathbf{E} &= \Delta\mathbf{M}_2^T\mathbf{M}_2\Delta^T - \mathbf{M}_1\mathbf{M}_2^T\mathbf{M}_2\Delta^T - \Delta\mathbf{M}_2^T\mathbf{M}_2\mathbf{M}_1^T \\ \mathbf{F} &= \mathbf{M}_2\Delta^T\Delta\mathbf{M}_2^T - \mathbf{M}_2\mathbf{M}_1^T\Delta\mathbf{M}_2^T - \mathbf{M}_2\Delta^T\mathbf{M}_1\mathbf{M}_2^T\end{aligned}$$

We can say that $\mathcal{U}$ contains the perturbed eigenvectors of $\mathbf{A}$ with perturbation $\mathbf{E}$, and $\mathcal{V}$ contains the perturbed eigenvectors of $\mathbf{B}$ with perturbation $\mathbf{F}$.

The first order eigenvector perturbation [22] of $\mathbf{U}$ and $\mathbf{V}$ are

$$\mathcal{U}_k = \mathbf{u}_k + \sum_{i=1,i\neq k}^{3}\frac{\mathbf{u}_i^T\mathbf{E}\mathbf{u}_k}{(\lambda_k - \lambda_i)}\mathbf{u}_i, \quad \mathcal{V}_k = \mathbf{v}_k + \sum_{i=1,i\neq k}^{3}\frac{\mathbf{u}_i^T\mathbf{F}\mathbf{v}_k}{(\lambda_k - \lambda_i)}\mathbf{v}_i \tag{13}$$

where the λs are the eigenvalues of $\mathbf{A}$. Rewriting (12),

$$\begin{aligned}(\mathbf{R}^* - \mathcal{R})^T(\mathbf{R}^* - \mathcal{R}) &= 2\mathbf{I} - \mathbf{V}\mathbf{U}^T\mathcal{R} - \mathcal{R}^T\mathbf{U}\mathbf{V}^T \\ &= 2\mathbf{I} - (\mathbf{V}+\delta\mathbf{V})(\mathbf{U}+\delta\mathbf{U})^T\mathbf{R}^* - \mathbf{R}^{*T}(\mathbf{U}+\delta\mathbf{U})(\mathbf{V}+\delta\mathbf{V})^T \\ &= -\delta\mathbf{V}\delta\mathbf{U}^T\mathbf{R}^* - \mathbf{R}^{*T}\delta\mathbf{U}\delta\mathbf{V}^T - \mathbf{V}\delta\mathbf{U}^T\mathbf{R}^* - \delta\mathbf{V}\mathbf{U}^T\mathbf{R}^* - \mathbf{R}^{*T}\mathbf{U}\delta\mathbf{V}^T - \mathbf{R}^{*T}\delta\mathbf{U}\mathbf{V}^T\end{aligned}$$

Thus

$$\begin{aligned}E((\mathbf{R}^* - \mathcal{R})^T(\mathbf{R}^* - \mathcal{R})) &= -E(\delta\mathbf{V}\delta\mathbf{U}^T)\mathbf{R}^* - \mathbf{R}^{*T}E(\delta\mathbf{U}\delta\mathbf{V}^T) \\ &\quad -\mathbf{V}E(\delta\mathbf{U}^T)\mathbf{R}^* - E(\delta\mathbf{V})\mathbf{U}^T\mathbf{R}^* - \mathbf{R}^{*T}\mathbf{U}E(\delta\mathbf{V}^T) - \mathbf{R}^{*T}E(\delta\mathbf{U})\mathbf{V}^T\end{aligned}$$

where $E(\delta\mathbf{V}\delta\mathbf{U}^T)$, $E(\delta\mathbf{U})$ and $E(\delta\mathbf{V})$ can be found by substituting $E(\mathbf{E})$ and $E(\mathbf{F})$ into (13).

D.2 Uncertainty in Translation

From Equation (6) and (11) we have

$$\sum_{i=1}^{l} w_{ti}(\mathbf{I} + \frac{\mathbf{n}_i\mathbf{n}_i^T}{(\mathbf{n}_i.\mathbf{m}_i)^2} - \frac{\mathbf{m}_i\mathbf{n}_i^T}{\mathbf{n}_i.\mathbf{m}_i} - \frac{\mathbf{n}_i\mathbf{m}_i^T}{\mathbf{n}.\mathbf{m}_i})\tilde{\mathbf{t}} = \sum_{i=1}^{l} w_{ti}(\mathbf{I} - \frac{\mathbf{n}_i\mathbf{m}_i^T}{\mathbf{n}_i.\mathbf{m}_i})(\mathbf{I} - \frac{\mathbf{m}_i\mathbf{n}_i^T}{\mathbf{n}_i.\mathbf{m}_i})(\tilde{\mathbf{a}}_i - \tilde{\mathbf{a}'}_i)$$

which can be written as

$$\tilde{\mathbf{t}} = \Phi^{-1}\sum_{i=1}^{l}\Theta_i(\tilde{\mathbf{a}}_i - \tilde{\mathbf{a}'}_i),$$

where

$$\begin{aligned}\Phi &= \sum_{i=1}^{l} w_{ti}(\mathbf{I} + \frac{\mathbf{n}_i\mathbf{n}_i^T}{(\mathbf{n}_i.\mathbf{m}_i)^2} - \frac{\mathbf{m}_i\mathbf{n}_i^T}{\mathbf{n}_i.\mathbf{m}_i} - \frac{\mathbf{n}_i\mathbf{m}_i^T}{\mathbf{n}.\mathbf{m}_i}) \\ \Theta_i &= w_{ti}(\mathbf{I} - \frac{\mathbf{n}_i\mathbf{m}_i^T}{\mathbf{n}_i.\mathbf{m}_i})(\mathbf{I} - \frac{\mathbf{m}_i\mathbf{n}_i^T}{\mathbf{n}_i.\mathbf{m}_i})\end{aligned}$$

Hence,

$$\begin{aligned}E(\tilde{\mathbf{t}}^T\tilde{\mathbf{t}}) &= E[\sum_{i=1}^{l}((\tilde{\mathbf{a}}_i - \tilde{\mathbf{a}'}_i)^T\Theta_i^T)\Phi^{-T}\Phi^{-1}\sum_{i=1}^{l}(\Theta_i(\tilde{\mathbf{a}}_i - \tilde{\mathbf{a}'}_i))] \\ &= E\sum_{i=1}^{l}[(\tilde{\mathbf{a}}_i - \tilde{\mathbf{a}'}_i)^T\Theta_i^T\Phi^{-T}\Phi^{-1}\Theta_i(\tilde{\mathbf{a}}_i - \tilde{\mathbf{a}'}_i)].\end{aligned}$$

Since the errors are independent, we have

$$E(\tilde{\mathbf{t}}^T\tilde{\mathbf{t}}) = \sum_{i=1}^{l}\{\sum_{pq}(\Theta_i^T\Phi^{-T}\Phi^{-1}\Theta_i)_{pq}(\Sigma_{ai,1})_{pq} + \sum_{pq}(\mathbf{R}^{*T}\Theta_i^T\Phi^{-T}\Phi^{-1}\Theta_i\mathbf{R}^*)_{pq}(\Sigma_{ai,2})_{pq}\}$$

E Line Fitting

A line can be represented by the following equation

$$\mathbf{r} = \mathbf{a} + k\mathbf{m}$$

or

$$\begin{pmatrix} x \\ y \\ z \end{pmatrix} = \begin{pmatrix} a_x \\ a_y \\ a_z \end{pmatrix} + k\begin{pmatrix} m_x \\ m_y \\ m_z \end{pmatrix}$$

where $(a_x, a_y, a_z)'$ is any point on the line and $(m_x, m_y, m_z)'$ is the direction of the line. Without any loss of generality, we could set $a_z = 0.0$ and $m_z = 1.0$ (although this is not true for lines that are parallel to the z-direction, we assume that the through plane direction is properly oriented such that no line is parallel to the z-plane). Thus the equation for a line is

$$\begin{pmatrix} x \\ y \end{pmatrix} = \begin{pmatrix} a_x \\ a_y \end{pmatrix} + z \begin{pmatrix} m_x \\ m_y \end{pmatrix}$$

For a particular z, we estimate the (x, y) component of the line. By repeating the procedure for a series of $(z_1, \ldots, z_n)$, we obtain $(x_1, \ldots, x_n)$ and $(y_1, \ldots, y_n)$. We could form the following equation for the x components

$$\begin{pmatrix} x_1 \\ \vdots \\ x_n \end{pmatrix} = \begin{pmatrix} 1 & z_1 \\ \vdots & \vdots \\ 1 & z_n \end{pmatrix} \begin{pmatrix} a_x \\ m_x \end{pmatrix} + \begin{pmatrix} e_{x,1} \\ \vdots \\ e_{x,n} \end{pmatrix} \tag{14}$$

where $(e_{x,1}, \ldots, e_{x,n})'$ are the estimation errors for the $(x_1, \ldots, x_n)'$. Based on the assumption that the estimation errors for each z are independent and have the same variance (which is true in most cases), (a_x, m_x) in (14) could be estimated by any standard linear regression technique [23]. Using the following notation:

$$\mathbf{x} = \begin{pmatrix} x_1 \\ \vdots \\ x_n \end{pmatrix}, \mathbf{Z} = \begin{pmatrix} 1 & z_1 \\ \vdots & \vdots \\ 1 & z_n \end{pmatrix},$$

the estimated values for (a_x, m_x) are

$$\begin{pmatrix} \hat{a}_x \\ \hat{m}_x \end{pmatrix} = (\mathbf{Z}^T\mathbf{Z})^{-1}\mathbf{Z}^T\mathbf{x}$$

and

$$\sigma^2_{a,x} = var(\hat{a}_x) = \sigma^2_x\{(\mathbf{Z}^T\mathbf{Z})^{-1}\}_{11} \tag{15}$$

$$\sigma^2_{m,x} = var(\hat{m}_x) = \sigma^2_x\{(\mathbf{Z}^T\mathbf{Z})^{-1}\}_{22} \tag{16}$$

where $\sigma^2_x = var(e_i)$ and $\{(\mathbf{Z}^T\mathbf{Z})^{-1}\}_{ij}$ refers to the (i, j) element of the matrix $(\mathbf{Z}^T\mathbf{Z})^{-1}$. We perform the same procedure for the y component of the line.

F Estimation of σ^2

In cases where $var(e)$ is unknown, we could use the following method to obtain an estimated σ^2 [23]. Since σ^2 is the expected squared value of an error, e_i, it is natural to use the simple squared value of the residuals. The vector of residual for the x component is

$$\begin{aligned} \hat{\mathbf{e}}_x &= \mathbf{x} - \hat{\mathbf{X}} \\ &= \mathbf{x} - \mathbf{Z}(\mathbf{Z}^T\mathbf{Z})^{-1}\mathbf{Z}^T\mathbf{x} \end{aligned}$$

Under the assumption that the errors are uncorrelated with constant variance σ^2_x, an unbiased estimate of σ^2_x is

$$\hat{\sigma}^2_x = \frac{\| \mathbf{x} - \hat{\mathbf{x}} \|^2}{n - p}$$

where p is the number of parameter (which is 2 in this case) and n is the data size. σ^2_y is estimated in a similar manner.

References

[1] W. E. L. Grimson, G. J. Ettinger, S. J. White, T. Lozano-Pèrez, and W. M. Wells III. An automatic registration method for frame-less stereotaxy, image guided surgery and enhance reality visualization. *IEEE Transaction on Medical Imaging*, 15(2):139–140, April 1996.

[2] T. Peters, B. Davey, P. Munger, R. Comeau, A. Evans, and A. Olivièr. Three dimensional multi-modal image-guidance for neurosurgery. *IEEE Transaction on Medical Imaging*, 15(2):121–128, April 1996.

[3] P. F. Hemler, T. S. Sumanaweera, P. A. van den Elsen, S. Napel, and J. Adler. A versatile system for multi-modality image fusion. *Journal of Image Guided Surgery*, 1:35–45, 1995.

[4] C. R. Maurer and J. M. Fitzpatrick. A review of medical image registration. In R.J. Maciunas, editor, *Interactive Image-Guided Neurosurgery*, chapter 3, pages 17–44. American Association of Neurological Surgeons, 1993.

[5] P. A. van den Elsen, E. D. Pol, and M. A. Viergever. Medical image matching - a review with classification. *IEEE Engineering in Medicine and Biology*, 12:26–39, March 1993.

[6] C. H. Yan *et al.* Registration of serial skeletal images for accurately measuring changes in bone density. Submitted to *43rd Annual Meeting, Orthopaedic Research Society*, 1996.

[7] E. F. Fitchard and P. A. Narayana. Two-dimensional registration of magnetic resonance brain images. *Medical Physics*, 21(8):1333–1338, August 1994.

[8] P. K. Banerjee and A. W. Toga. Image alignment by integrated rotational and translational transformation matrix. *Physics of Medicine and Biology*, 39:1969–1988, 1994.

[9] D. Hill and D. J. Hawkes *et al.* Registration of MR and CT images for skull base surgery using point like anatomical features. *British Journal of Radiology*, 64:1030–1035, 1991.

[10] A. Evans, S. Marret, L. Collins, and T. Peters. Anatomical-functional correlative analysis of the human brain using three dimensional imaging system. *SPIE*, 1092:264–274, 1989.

[11] P. F. Hemler, T. S. Sumanaweera, P. A. van den Elsen, S. Napel, J. Drace, and J. Adler. A quantitative comparison of residual error for three different multi-modality registration techniques. *Information Processing in Medical Imaging*, February 1995.

[12] P. F. Hemler, T. S. Sumanaweera, P. A. van den Elsen, and S. Napel. Registration error quantification of a surface-based multi-modality image fusion system. *Medical Physics*, 22(7):1049–1056, July 1995.

[13] R. P. Woods, J. C. Mazziotta, and S. R. Cherry. MRI-PET registration with automated algorithm. *Journal of Computer Assisted Tomography*, 17(4):536–546, July/August 1993.

[14] L. Lemieux and N. D. Kitchen *et al.* Voxel-based localization in frame-based and frame-less stereotaxy and its accuracy. *Medical Physics*, 21(8):1301–1310, August 1994.

[15] Y. Ge and M. Fitzpatrick *et al.* Retrospective registration of pet and mr brain images: An algorithm and its stereotactic validation. *Journal of Computed Assisted Tomography*, 18(5):800–810, September 1994.

[16] P. A. Van den Elsen *et al.* Automatic registration of CT and MR brain images using correlation of geometrical features. *IEEE Transactions on Medical Imaging*, 14(2):384–396, June 1995.

[17] J. West and J. M. Fitzpatrick *et al.* Comparison and evaluation of retrospective inter-modality image registration techniques. *SPIE*, 2710:332–347, 1996.

[18] J. Zhang and M. F. Levesque *et al.* Multi-modality imaging of brain structures for stereotactic surgery. *Radiology*, 175:435–441, 1990.

[19] T. M. Peters and J. A. Clark *et al.* Integrated stereotaxtic imaging with CT, MR imaging, and digital subtraction angiography. *Medical Physics*, 161:821–826, 1986.

[20] C. R. Crawford. Personal communication, 1996.

[21] G. H. Golub. *Matrix Computations.* Johns Hopkins University Press, 2nd edition, 1983.

[22] J. H. Wilkinson. *The Algebraic Eigenvalue Problem.* Oxford, Clarendon Press, 1st edition, 1965.

[23] S. Weisberg. *Applied Linear Regression.* John Wiley & Sons, 2nd edition, 1985.

Registration of Serial Skeletal Images for Accurately Measuring Changes in Bone Density

Chye Hwang Yan, G.S. Beaupre *, R.T. Whalen**, S. Napel ***
Department of Electrical Engineering, Stanford University, CA 94305, USA

Relevance to Musculoskeletal Condition: The non-invasive determination of changes in bone mass is valuable as a clinical assessment tool in a variety of settings. Examples include: evaluating the efficacy of drug therapy in the treatment of osteoporosis; understanding local bone adaptation in response to exercise intervention; and assessing the progression of bone loss with skeletal disease.

Introduction: The accurate measurement of bone apparent density from Computed Tomography (CT) requires a consideration of image noise, marrow presence and beam hardening. Non-invasive measurement of changes in bone apparent density (grams/cm3) further necessitates imaging the same skeletal site at different times and registering the serial images. Mis-registration can introduce errors, particularly when density gradients are high. The effect of mis-registration errors generally increases as the size of the volume of interest (VOI) decreases. For this reason and because of image noise relatively large VOI's (3000-4000 mm3) are typically analyzed [1,2].

We have developed a semi-automated, 3D, surface-based registration technique that does not require the use ofan external frame or fiducial markers. The accuracy of our non-invasive registration technique is comparable to that which can be obtained using standard invasive approaches (e.g., skeletal pins and frames). The objective of this study was to assess the accuracy and precision of repeated registration of the human calcaneus whe n imaged with a clinical CT scanner.

Methods: Excised human calcanei were secured within a custom-made fiducial frame, referred to as a "tiger cage" (Fig. 1). The tiger cage/calcaneus was scanned in different orientations using a GE HiSpeed Advantage CT scanner. Scanning technique consisted of: helical mode; 120 kVp; 240 mA; 1.0 mm slice thickness; pitch = 1.7, scan field of view = 250 mm; display field of view = 120P130 mm; standard reconstruction algorithm. Using a 512 x 512 reconstruction matrix, the in-plane pixel size was approximately 0.25 mm. Reconstructions were done every 0.5 mm in the through-plane direction. To examine the effects of image noise and contrast, the tiger cage/calcaneus was scanned both in air and in water contained within a 240 mm diameter, thin-walled (12.7 mm) plexiglass cylinder.

We have recently developed an improved gold standard [3] that we used to assess the accuracy of our new surface-based registration of the calcaneus. We determined registration accuracy by: 1) obtaining a gold standard transformation for the tiger cage between pairs of scans; 2) obtaining a transformation for the calcaneus using surface points only (200,000 to 300,000 points per calcaneus); 3) transforming all calcaneus voxels using both the gold standard and the calcaneus transformations; 4) calculating the distance (error) between corresponding voxels in the two transformed calcaneus images.

Results: Shown in Table 1 are the registration errors for the calcaneus scanned in air and scanned in water. Note that the average errors in air and water are similar and sub-pixel in magnitude.

Discussion: We have developed a highly accurate frameless registration technique for use in determining changes in bone density. The average error throughout the volume is sub-pixel in magnitude. It should be noted, however, that our registration errors are spatially correlated; highest accuracy exists near the centrum of the calcaneus. To our knowledge this new technique permits accurate registration of bone volumes an order of magnitude smaller than previously possible using clinical CT scanners. The technique is robust in the presence

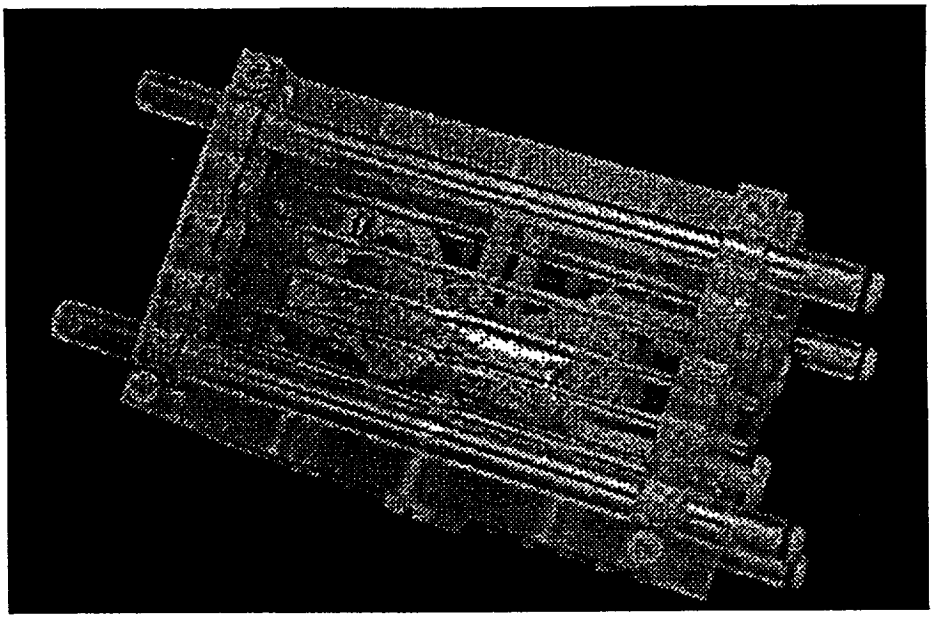

Figure 1: Calcaneus within tiger cage.

	Minimum Error	Average Error	Maximum Error
Calcaneus in air (4 Registrations)	0.002 (±0.005)	0.180 (±0.017)	0.360 (±0.029)
Calcaneus in water (4 Registrations)	0.040 (±0.020)	0.200 (±0.060)	0.400 (±0.110)

Table 1: Registration Error (mm)

of noise with minimal degradation of registration accuracy when scanning with a water bolus. Furthermore, by using surface points only, the accuracy of registration is independent of changes in bone apparent density.

Highly accurate and precise registration is an essential component for non-invasive monitoring of changes in local volumetric bone density. Using this newly developed registration technique it will be possible, for example, to monitor more accurately osteoporosis progression and treatment in both large and small regions using a clinical CT scanner. In particular, the ability to measure bone changes in small regions allows one to examine relationships between remodeling rates and local bone morphological parameters such as apparent density and related variables such as bone specific surface area.

References: [1] Klotz et al. Trans. Med. Imaging, 371P376, 1989; [2] Tanno et al. Bone, 239P247, 1996; [3] Yan et al., accepted 1996 Radiological Soc. N. Amer.

Acknowledgments: This work was supported by the Dept. of Veterans Affairs (B802PRA), NASA Ames Research Center (NCC2P5088), NIH (P41PRRP09784), Stanford University Department of Radiology and the Lucas Foundation. We would like to thank Laura Logan for her technical assistance.

Additional Affiliations
* Rehabilitation R&D Center, VA Palo Alto, CA. ** Life Sciences Div., NASA Ames Res. Ctr., Mt. View, CA. *** Dept. Radiology, Stanford University, Stanford, CA.

Precise and Accurate Gold Standard for Multimodality and Serial Registration Method Evaluations

Chye Hwang Yan, G.S. Beaupre, R.T. Whalen, T.S. Sumanaweera, S. Napel
Department of Electrical Engineering, Stanford University, CA 94305, USA

Purpose: The accuracy of a registration method is usually determined by using the registration of an attached stereotactic frame as the gold standard. Existing frame registration techniques are: (1) matching each 2D slice separately to an N-bar model (2) using 2 detected N-bars (6 per frame) as the coordinate system. These techniques assume a precise frame model and only utilize partial 3D information. We propose a technique that assumes only linear structures (rods) in the frame and utilizes all 3D information.

Materials and Methods: Our technique fits lines to all linear structures in each data set and registers them using a closed form solution. We obtained CT scans (0.24x0.24x1.00mm^3 voxels) of a frame at 8 orientations. We performed 28 registrations between scans using existing and proposed techniques. We defined registration error as the maximum deviation between registered corresponding rods.

Results: Registration errors (average, maximum) for the existing 2D and 3D techniques were (0.18mm, 0.22mm) and (0.08mm, 0.11mm) respectively. The proposed method reduced the error to (0.035mm, 0.04mm).

Conclusion: The proposed technique produces more accurate registration without requiring any knowledge of the frame geometry. It is used to evaluate our new surface registration technique, for high-resolution QCT, which has an accuracy comparable to existing gold standards.

Take Home Points: (1) accurate registration with simple frame. (2) global minimum registration.

References

[1] Terence M. Peters, "Integrated Stereotaxic Imaging with CT, MR Imaging, and Digital Subtraction Angiography", *Medical Physics*, December 1986, pp 821-826.

[2] Jingxi Zhang, "Multimodality Imaging of Brain Structures for Stereotactic Surgery", *Radiology*, May 1990, pp 435-441.

[3] Roger P. Woods, "MRI-PET Registration with Automated Algorithm", *Journal of Computer Assisted Tomography*, July 1993, pp 536-546.